applied sciences

MDPI

*Article*

# Influence of Lateral Multistage Unloading Intensity on Mechanical Properties of Reconstituted Coastal Soils Containing Silty Particles

**Changqing Xia [1,2,3], Fanli Meng [4,*], Min Zhu [1,2,3], Yan Tang [4] and Chengyuan Lu [4]**

1 College of Civil and Transportation Engineering, Shenzhen University, Shenzhen 518061, China; xiacq09@szu.edu.cn (C.X.); zhuminfnf@szu.edu.cn (M.Z.)
2 Underground Polis Academy, Shenzhen University, Shenzhen 518061, China
3 Key Laboratory of Coastal Urban Resilient Infrastructures (MOE), Shenzhen University, Shenzhen 518061, China
4 College of Civil Engineering, Zhejiang University of Technology, Hangzhou 310023, China; tangyan199407@163.com (Y.T.); zgdlucy@sina.com (C.L.)
* Correspondence: zgdmfl@zjut.edu.cn

**Abstract:** The unclear understanding of the mechanical behavior of soil under unloading conditions is a significant reason for the frequent occurrence of accidents and difficulties in the deformation control of foundation pit engineering in coastal areas. This paper discusses the effect of multistage unloading intensity on the mechanical properties of reconstituted coastal soils containing silty particles through a series of laboratory tests, namely, the CU triaxial, bender-element, and permeability tests. Results indicate that, with an increase in unloading intensity, the shear strength and stiffness parameters decrease, while permeability slightly increases. The effect of unloading intensity on the mechanical properties of silt and mucky silty clay is more pronounced. Additional consideration should be given to the effect of a single excavation depth on the mechanical properties of fine-grained soil in foundation pit engineering in order to ensure the stability of the surrounding soil and the safety of adjacent structures.

**Keywords:** silty soil; lateral unloading; multistage unloading intensity; mechanical properties



**Citation:** Xia, C.; Meng, F.; Zhu, M.; Tang, Y.; Lu, C. Influence of Lateral Multistage Unloading Intensity on Mechanical Properties of Reconstituted Coastal Soils Containing Silty Particles. *Appl. Sci.* **2022**, *12*, 3651. https://doi.org/10.3390/app12073651

Academic Editor: Daniel Dias

Received: 10 March 2022
Accepted: 30 March 2022
Published: 5 April 2022



## 1. Introduction

Urban issues such as land resource scarcity and traffic congestion resulting from rapid city expansion are a significant threat to the sustainable development of coastal cities. The development of high-quality underground spaces is an effective way to address this issue [1]. Due to the complex engineering properties of soil, foundation pit excavation in coastal areas has resulted in fatal accidents [2]. Foundation excavations conducted without adequate safeguards also result in significant deformation or even structural damage to adjacent underground structures, including shield tunnels and metro stations [3–5]. When evaluating the safety and environmental impact of foundation engineering, the mechanical properties and parameters of soil are typically determined through loading tests, which include conventional triaxial and pressure-meter tests [6,7]. The excavation of foundation pits is a common unloading problem, and extensive research demonstrates that the mechanical properties of soil are inextricably linked to the stress path [8,9]. As a result, the difference in soil properties between loading and unloading stress paths may result in unpredictable calculation errors in foundation engineering. It is thus critical to have a thorough understanding of the stress and deformation characteristics of coastal soil during unloading.

Numerous experimental studies on the mechanical properties of soils subjected to unloading paths have confirmed that the unloading process has a significant effect on the strength and stiffness properties of the soil. Unloading ratio $R$ is frequently used to

represent various unloading stress paths. It is defined as the ratio of the absolute value of vertical stress unloading ($|\Delta\sigma_1|$) to the absolute value of horizontal stress unloading ($|\Delta\sigma_3|$). $R$ is zero for axial unloading and tends to infinity for lateral unloading. Triaxial compression tests on soft soils demonstrate that, in comparison to axial loading, soil samples subjected to unloading stress paths exhibit decreased shear strength and a smaller initial tangent modulus [10,11]. Huang et al. [12] investigated the mechanical properties of marine sedimentary soft soils in relation to pore pressure and unloading ratio. Results indicate that increased pore pressure significantly reduces unloading strength, particularly cohesion. Zheng et al. [13,14] conducted a series of triaxial CU and CD tests on marine silty clay subjected to unloading stress paths. Total shear strength under drained and unloaded conditions was greater than that in conventional triaxial tests, but effective shear strength was not significantly different. Under undrained and unloaded conditions, the initial tangent modulus was directly proportional to the initial confining pressure. Zhang et al. [15] conducted unloading stress path drainage tests on silty clay under $K_0$ consolidation. The stress–strain relationship was quite different under various unloading stress paths. Ding et al. [16] investigated the deformation properties of silty clay during unloading and loading in Guangzhou. The results of tests conducted on silty clay and mucky soil under axial and lateral unloading stress paths indicated that the failure modes of axial and lateral unloading samples are distinct, and that the stress–strain relationship is highly dependent on consolidation stress, plastic index, and confining pressure. However, because foundations are typically excavated layer by layer, the soil unloading process occurs in stages, resulting in a significantly different unloading intensity levels. It is unknown how unloading intensity affects the mechanical properties of coastal soil.

Over the last few decades, the nonlinear effect of strain on soil stiffness has been extensively investigated. Very small strain stiffness is believed to be a fundamental property of all geotechnical materials, and it is critical for properly evaluating excavation-induced deformation [17,18]. The normalized shear modulus and shear strain relationships of clays, silts, sands, and gravels are established using a variety of laboratory and in situ test methods, including the bender element test, resonant column test, torsional shear, cyclic triaxial test, cross-hole test, spectral analysis of surface waves, suspension logger, and seismic cone penetration test [19,20]. Stress state [21,22], loading history [23], and strain rate all have a significant effect on the small-strain stiffness [24]. Although many scholars are interested in the small-strain shear stiffness of soil under unloading conditions, the small-strain properties of soil under various lateral unloading intensity require additional research.

In this paper, the mechanical properties of silt, silty sand, and mucky silty clay are investigated using laboratory tests including the CU triaxial, bender-element, and permeability tests to determine the effect of foundation pit excavation on soil properties, and to provide a theoretical basis for the determination of soil parameters.

## 2. Experimental Methods

During foundation pit excavation and basement construction, as shown in Figure 1, the stress paths of surrounding soil are unloaded and reloaded, respectively. Thus, the triaxial, bender-element, and permeability tests are used to investigate the mechanical properties of three distinct types of reconstituted coastal soils containing silty particles, namely, silt, silty sand, and mucky silty clay at various lateral unloading intensity levels.

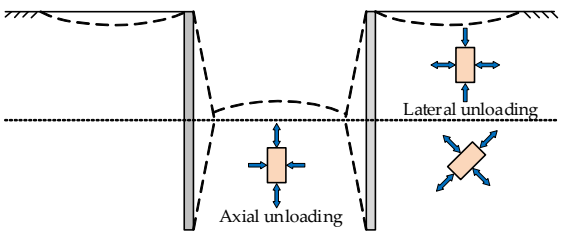


**Figure 1.** Unloading affected area of foundation pit excavation.

### 2.1. Soil

The soil sampled for this study came from a foundation pit in eastern Hangzhou, China as shown in Figure 2. The particle composition of soil determined by sieve analysis is summarized in Table 1. Silt contains 89.52% silt particles. Silty sand has a coarser particle size and contains 66.68% fine sand. Mucky silty clay is primarily composed of silt particles (67.76%), but also contains a significant amount of clay particles (30.08%).


**Figure 2.** Sampling sites.

**Table 1.** Particle size distribution of soil.

| Particle Size | Silt | Silty Sand | Mucky Silty Clay |
|---|---|---|---|
| Fine sand (0.25–0.075 mm) (%) | 2.48 | 66.68 | 2.16 |
| Silt (0.075–0.005 mm) (%) | 89.52 | 27.32 | 67.76 |
| Clay (<0.005 mm) (%) | 8.00 | 6.00 | 30.08 |

To maintain the uniformity of the reconstituted soil sample, the dry density and water content of silt, silty sand, and mucky silty clay soil samples were kept the same at 1.46 g/cm$^3$ and 22%, respectively. Water content, density, specific gravity, void ratio, liquid limit, plastic limit, and plastic index of the reconstituted soil are listed in Table 2. The void ratio and plastic index of mucky silty clay were greater, while silt and silty sand had similar physical properties.

**Table 2.** Physical properties of soil.

| Physical Properties | Silt | Silty Sand | Mucky Silty Clay |
|---|---|---|---|
| Water content $w$ (%) | 22 | 22 | 22 |
| Density $\rho$ (g/cm$^3$) | 1.78 | 1.78 | 1.78 |
| Dry density $\rho_d$ (g/cm$^3$) | 1.46 | 1.46 | 1.46 |
| Specific gravity $G_s$ | 2.72 | 2.70 | 2.73 |
| Void ratio $e$ | 0.79 | 0.765 | 1.27 |
| Liquid limit $w_L$ (%) | 31.42 | 29.60 | 39.60 |
| Plastic limit $w_P$ (%) | 24.63 | 20.20 | 23.10 |
| Plastic index $I_p$ | 6.79 | 9.40 | 16.50 |

### 2.2. Unloading and Reloading Stress Paths

Triaxial, bender-element, and permeability tests were performed on the three reconstituted soils, and the preparation methods for soil samples and stress paths for the three types of tests were similar. To simulate the initial state and excavation process of the foundation pit, different unloading and reloading stress paths were designed in the experiment, with lateral unloading intensity as the primary variable.

For simulating more than 20 m deep foundation pit excavation, consolidation confining pressure was set to 150 kPa, consolidation ratio was set to 1.0, and unloading capacity was set to 90 kPa. Table 3 details the specific test procedure. Group A focused on the shear properties of soil under a conventional triaxial path. Group B measured the mechanical properties under a lateral unloading path with different multistage unloading intensity to consider the effect of staged construction excavation. Group C determined the mechanical properties in the path of unloading and reloading with different unloading intensity levels to take account of the effect of building work after excavation is finished.

**Table 3.** Test scheme.

| Type | Number | Stress Paths (kPa) |
|---|---|---|
| Conventional CU triaxial test | A−0 | 150 |
| CU triaxial tests under lateral unloading stress paths | B−1 | 150→140→130→120→110→100→90→80→70→60 |
| | B−2 | 150→130→110→90→70→60 |
| | B−3 | 150→120→90→60 |
| CU triaxial tests under lateral unloading–reloading stress paths | C−1 | 150→140→130→120→110→100→90→80→70→60→150 |
| | C−2 | 150→130→110→90→70→60→150 |
| | C−3 | 150→120→90→60→150 |

### 2.3. Experimental Procedures

#### 2.3.1. Triaxial Test

1. Sample Preparation

A solid cylinder with a diameter of 50 mm and a height of 100 mm was prepared for this test. The compaction method was chosen in accordance with the Specification of Soil Test (GB/T50123-2019). Soil samples were divided into five parts. Each component was poured layer by layer into the sample preparation device and then pressed to the specified height according to the designed water content and density. The upper plane of the previous layer was scraped away, and the next layer of soil was added and compacted to ensure the uniformity of the soil samples.

2. Saturation

The soil sample was loaded into the vacuum pumping cylinder and then saturated using the vacuum saturation technique. The vacuum cylinder was connected to the air extraction pump to maintain negative pressure of 100 kPa for one hour, and airless water was then slowly injected from the bottom of the soil sample. After the sample had been completely submerged in water, drainage was stopped, and air extraction continued for another half an hour. Valves were then completely closed to keep the sample submerged in water.

3. Consolidation

Isotropic consolidation was used in the test. After loading the soil sample, the pressure chamber was installed. Then the sample was contacted and zeroed axially, and the confining pressure was added to the specified value. Consolidation began once the pore water pressure had reached a stable level, and the check saturation had met the specified requirements. Consolidation was completed when the pore water pressure of the sample had dropped by more than 95%.

4. Unloading and reloading

After initial consolidation, the lateral stress of the sample was unloaded in stages in accordance with the test scheme. The sample was consolidated and then unloaded onto the next stage following each stage of unloading. Following unloading, the reloading process was also incrementally loaded until the target value had been reached. All loading and unloading rates were set at 1 kPa/min.

5. Three-dimensional shear test

Consolidated undrained shear tests were performed on soil samples. In order to properly compare the mechanical properties of the three soils and reduce the test error, shear rate was set at 0.5%/min for silt, silty sand, and mucky silty clay. We monitored and recorded axial pressure, confining pressure, axial strain, and pore pressure until the axial strain had reached 15%.

#### 2.3.2. Bender-Element Test

A bender-element was is carried out to obtain the small-strain shear module of silt. In order to accurately measure the shear wave velocity and avoid interference from other factors, the sine wave pulse signal was selected. The period of the sine wave was set to 0.2 ms, and the amplitude was set to 14 V (maximum). The shear wave velocity and shear modulus were calculated by the following equations.

$$v_s = h/t_s, \quad (1)$$

$$G_{max} = \rho v_s^2, \quad (2)$$

where $t_s$ is the transmission time, $h$ is the height of soil sample, $\rho$ is the density of soil, $v_s$ is the shear wave velocity, and $G_{max}$ is the small-strain shear modulus.

The test steps are as follows:

1. Installation

The saturated soil sample was covered with rubber film and slowly placed on the pressure chamber base with the bender element receiving device installed. At that time, the bender-element launcher was installed on the top of the sample cap. When installing the device, the upper and lower ceramic wafers should be parallel or the electrical signal cannot be captured. The installed sample is shown in Figure 3.

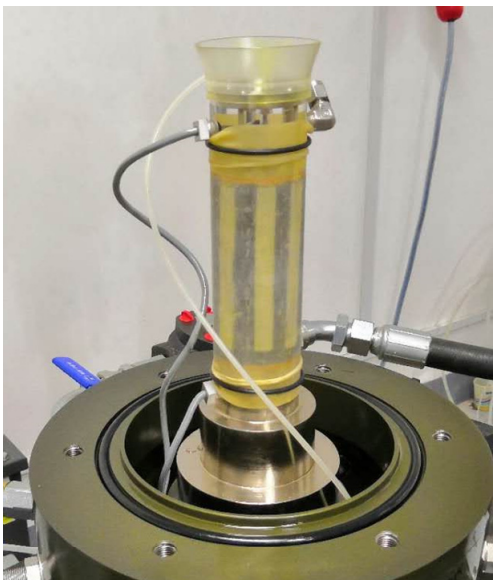

**Figure 3.** Installation of bender element.

2. Initial measurement

The phase of the transmitting curve should be the same as that of the receiving curve. As shown in Figure 4, the red curve was the emission curve, and the green curve was the reception curve. Transmission time and the shear wave velocity were automatically calculated by the computer.

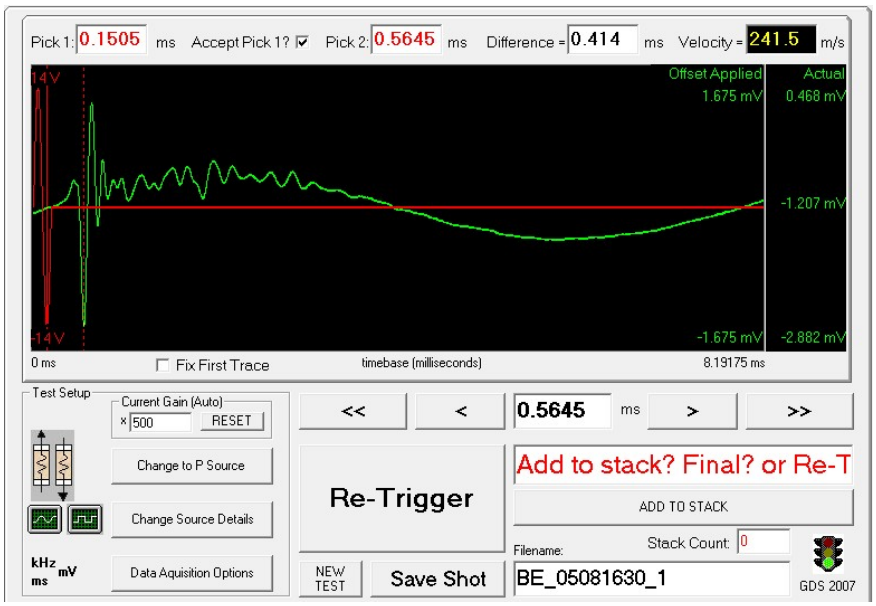


**Figure 4.** BES software interface display diagram.

3. Consolidation

Soil samples were consolidated according to the conventional originally designed triaxial, unloading, and unloading–reloading stress paths.

4. Bender-element test

After the soil samples had been consolidated, the transmission time of shear wave velocity was measured, and the shear modulus of soil samples was calculated by Equations (1) and (2).

2.3.3. Permeability Test

1. Installation

Soil samples used in the permeability tests were the same as those in the triaxial tests. The saturated soil sample was covered with rubber and slowly placed on the base of the pressure chamber. The permeability module of GDSLAB software was selected for the test.

2. Consolidation

Soil samples were consolidated according to the conventional originally designed triaxial, unloading, and unloading–reloading stress paths.

3. Permeability test

Water pressure difference was applied to allow for the sample to seep after unloading or unloading–reloading. The permeability coefficient of the sample was obtained when the seepage had been completed.

## 3. Results and Discussion

### *3.1. Deviator Stress–Strain Curves and Shear Strength Parameters*

The deviator stress–strain curves of silt, silty sand, and mucky silty clay under various stress paths are shown in Figure 5, and the deviator stress at 15% axial strain is summarized in Table 4. Silt and silty sand have comparable shear strength, but mucky silty clay has

much lower shear strength due to its high clay particle content. The deviator stress for Group B was less than the deviator stress for Groups A and C. This was mainly because the confining pressure of Group B (60 kPa) was smaller than the confining pressure of Groups A and C (150 kPa). The difference in deviator stress between Groups B and A was much smaller for mucky silty clay, indicating that the influence of confining pressure on the shear properties of mucky silty clay is not readily apparent due to its high void ratio and clay particle content.

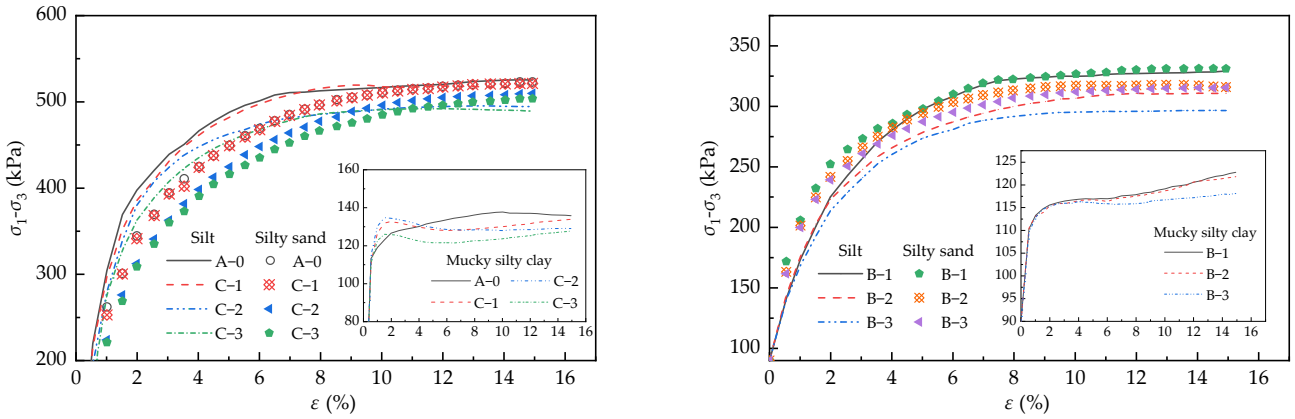


**Figure 5.** Deviator stress–strain relationship of soil under different stress paths. (**a**) Groups A and C; (**b**) Group B.

**Table 4.** Final deviator stress of soil under different stress paths (Unit: kPa).

| Stress | Soils | Stress Path | | | | | | |
|---|---|---|---|---|---|---|---|---|
| | | A−0 | B−1 | B−2 | B−3 | C−1 | C−2 | C−3 |
| $(\sigma_1-\sigma_3)_f$ (kPa) | Silt | 525.35 | 329.14 | 310.63 | 296.5 | 517.47 | 494.22 | 489.18 |
| | Silty sand | 523.08 | 331.06 | 315.86 | 315.45 | 521.34 | 509.74 | 503.64 |
| | Mucky silty clay | 135.84 | 122.74 | 121.80 | 118.12 | 133.93 | 129.04 | 127.80 |

Under the unloading path, as unloading intensity increased, the deviator stress of the three soils gradually decreased. When the single unloading intensity was 10 kPa (C−1), the deviator stress curves of silt and silty sand were almost identical to the conventional triaxial curve, indicating that low unloading intensity had little effect on the shear strength of the two soils. For mucky silty clay, although the final deviator stress is nearly identical, the deviator stress under the unloading–reloading path showed characteristics of first increasing and then decreasing.

The final deviator stress at 15% axial strain is summarized in Table 4. The normalized deviator stress–unloading intensity curves for Group B and C tests are shown in Figure 6, where Group B used B−1 as a reference value and Group C used the conventional triaxial A−0 as a reference value. Increased unloading intensity had the greatest effect on the deviator stress of silt. When unloading intensity was set at 30 kPa, the deviator stress of silt was reduced by 10% under the unloading path, and by 7% under the unloading reloading path. The variation law of the deviator stress of the three soils with unloading intensity is consistent under the unloading–reloading path. When unloading intensity was low, deviator stress reduction was not readily apparent. With increasing unloading intensity, the deviator stress rapidly decreased at first and then slowed down. In practical engineering, although the stress level of the soil is restored following foundation pit excavation and structural construction, close attention should be paid to the effect of the unloading–reloading stress path on the shear strength of the soil.

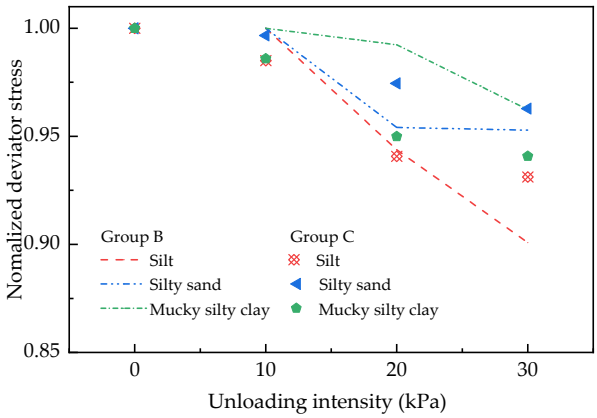


**Figure 6.** Normalized deviator stress–unloading intensity relationship of three soils under different stress paths.

The shear strength parameters of reconstituted silt, silty sand, and mucky silty clay in various stress paths are shown in Table 5. In comparison to conventional triaxial test, the lateral unloading test significantly reduces the shear strength parameters, including effective cohesion $c'$ and internal friction angle $\varphi'$. Similar tests were carried out using clay of low plasticity, and results showed that $c'$ decreased while $\varphi'$ increased in the unloading path [25]. Effective cohesion $c'$, internal friction angle $\varphi'$, and shear strength decreased as lateral unloading intensity increased.

**Table 5.** Shear strength indicators of soil under different unloading intensity levels.

| Properties | Soils | Stress Path | | | | | | |
|---|---|---|---|---|---|---|---|---|
| | | A−0 | B−1 | B−2 | B−3 | C−1 | C−2 | C−3 |
| Cohesive pressure $c'$ (kPa) | Silt | 8.66 | 1.16 | 1.1 | 0.98 | 8.55 | 8.12 | 7.83 |
| | Silty sand | 6.84 | 0.24 | 0.23 | 0.19 | 6.77 | 6.55 | 6.38 |
| | Mucky silty clay | 1.24 | 0.5 | 0.44 | 0.36 | 1.07 | 0.62 | 0.59 |
| Friction angle $\varphi'$ (°) | Silt | 36.35 | 28.71 | 28.56 | 26.69 | 35.5 | 35.3 | 35.26 |
| | Silty sand | 37.36 | 29.82 | 29.01 | 28.94 | 36.05 | 35.7 | 35.63 |
| | Mucky silty clay | 4.5 | 1.81 | 1.59 | 1.52 | 4.39 | 4.35 | 3.83 |
| Shear strength $\tau$ (kPa) | Silt | 119.05 | 83.32 | 82.75 | 76.39 | 115.54 | 114.32 | 113.87 |
| | Silty sand | 121.36 | 86.22 | 83.41 | 83.13 | 115.95 | 114.34 | 113.89 |
| | Mucky silty clay | 13.05 | 5.24 | 4.6 | 4.34 | 12.59 | 12.03 | 10.63 |

For unloading–reloading samples, the shear strength of the sample was restored due to the reloading process, but they could not reach their initial values under the same stress state as in the conventional triaxial test. Effective cohesion $c'$, internal friction angle $\varphi'$, and shear strength all slightly decreased as lateral unloading intensity increased.

### *3.2. Pore Pressure*

Figure 7 illustrates the development of pore pressure in soil samples subjected to various stress paths. The pore pressure development of silt and silty sand was similar. Pore pressure rapidly increased and then decreased in the stress path of Groups A and C. At first, the soil sample showed shear contraction and then exhibited shear dilation. For Group B's lateral unloading stress path, pore pressure had no obvious growth but continuously decreased. In the unloading path, as unloading intensity increased, the final pore water pressure decreased, and silty sand had a greater decline. The final pore pressure of silty sand decreased with increasing unloading intensity in the unloading–reloading path. The final pore pressure of silt decreased slightly, but peak pore pressure was significantly lower than that under a conventional triaxial path.

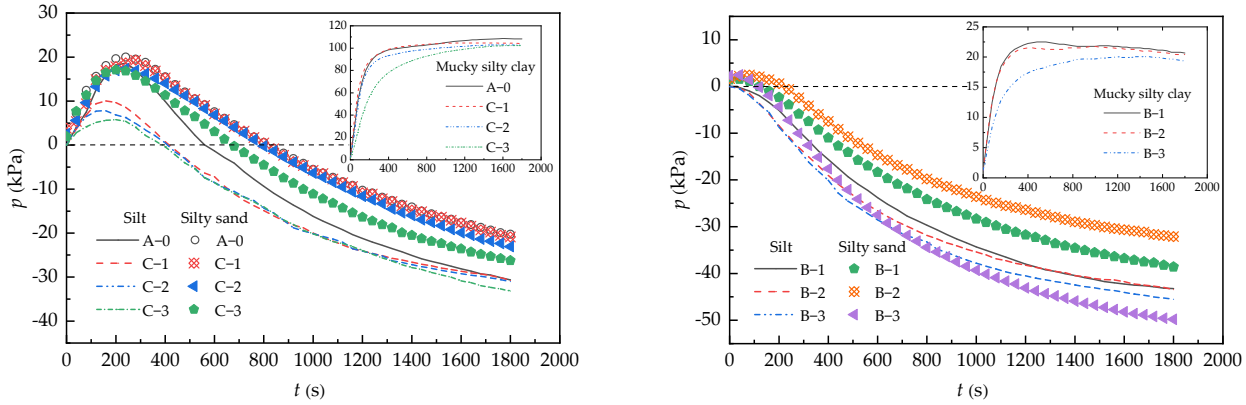


**Figure 7.** Pore pressure development of different soils under different stress paths. (**a**) Groups A and C; (**b**) Group B.

Pore pressure development takes on some distinct characteristics in mucky silty clay. Pore pressure is always positive under different stress paths. Under the unloading path, the pore pressure of silty clay initially increased and then slightly decreased. However, pore pressure continued to rise in the unloading–reloading path. As the final pore pressure of mucky silty clay slightly decreased with the increase in unloading intensity, growth rate significantly slowed down when unloading intensity was relatively high.

### *3.3. Normalization Analysis of Stress–Strain Curves*

The normalization of stress–strain curves is an important way to study the mechanical properties of soil. A hyperbolic function is widely used to express the stress–strain relationship of cohesive soil in the CU triaxial test [26]:

$$\sigma_1 - \sigma_3 = \varepsilon_1/(b + a\varepsilon_1), \tag{3}$$

which can be rewritten as

$$\varepsilon_1/(\sigma_1 - \sigma_3) = (b + a\varepsilon_1), \tag{4}$$

where $\sigma_1 - \sigma_3$ is deviator stress, $\varepsilon_1$ is axial strain, and $a$ and $b$ are two parameters of the hyperbolic function.

As shown in Equation (4), there was a linear relationship between $\varepsilon_1/(\sigma_1 - \sigma_3)$and $\varepsilon_1$. The intercept and slope of the line are $a$ and $b$, respectively. The physical meaning of $1/a$ and $1/b$ is the ultimate strength of soil and the initial modulus.

For the unloading stress path, initial deviator stress $\sigma_{1c} - \sigma_{3c}$ needed to be subtracted in Equation (4) [12], which is rewritten as

$$\varepsilon_1/[(\sigma_1 - \sigma_3) - (\sigma_{1c} - \sigma_{3c})] = (b + a\varepsilon_1), \tag{5}$$

The stress–strain curves of reconstituted Hangzhou silt under different stress paths were hyperbolic; thus, Equations (4) and (5) were used to fit curves for normalization analysis of the stress–strain relationship.

Figure 8 shows the normalized stress-strain relationship. R-squared values rangedfrom 0.9908 to 0.9998, which proves that the hyperbolic model is suitable for the normalization of the test results. Table 6 summarizes normalized curve parameters $a$ and $b$, and initial modulus $E_0$ under different stress paths. The $a$ and $b$ values of the three soils were greater in the unloading path, indicating that the ultimate deviator stress and initial elastic modulus were less than those under the two other paths. In the unloading–reloading path, when unloading intensity was 10 kPa, the $a$ and $b$ parameters were nearly identical to those of the conventional triaxial test for silt and silty sand. The $a$ and $b$ values of silt and silty

sand increased as unloading intensity increased, indicating that the ultimate deviator stress and initial modulus decreased. The relationship between normalized initial modulus and unloading intensity in different paths is shown in Figure 9, where Group B tests used B−1 data as a reference, and Group A and C tests used A−0 data as a reference. Unloading intensity had a greater effect on the initial modulus of silt in the unloading path. When unloading intensity increased to 30 kPa, the initial modulus of Groups B and C decreased by 19% and 23%, respectively. In the unloading–reloading path, the initial elastic modulus of mucky silty clay increased by 56% with the increase in unloading intensity.

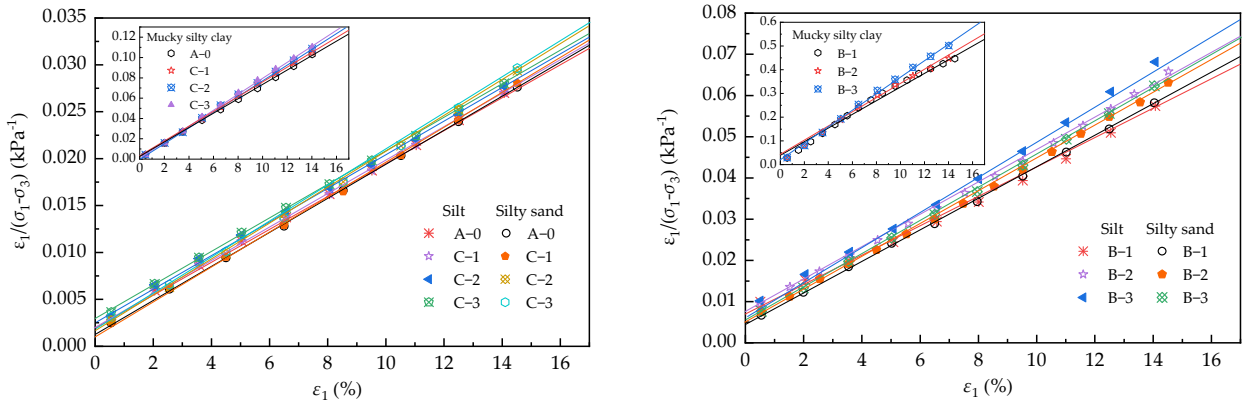


(**a**) (**b**)

**Figure 8.** Normalized stress–strain curves under different stress paths. (**a**) Groups A and C; (**b**) Group B.

**Table 6.** Normalized parameters under different stress paths.

| Parameters | Soils | Stress Path | | | | | | |
|---|---|---|---|---|---|---|---|---|
| | | **A−0** | **B−1** | **B−2** | **B−3** | **C−1** | **C−2** | **C−3** |
| $a$ (kPa$^{-1}$) | Silt | 0.0017 | 0.0035 | 0.004 | 0.0043 | 0.0017 | 0.0018 | 0.0018 |
| | Silty sand | 0.0018 | 0.0038 | 0.0039 | 0.004 | 0.0018 | 0.0019 | 0.0019 |
| | Mucky silty clay | 0.0072 | 0.0353 | 0.0359 | 0.0360 | 0.0075 | 0.0077 | 0.0079 |
| $b$ (MPa$^{-1}$) | Silt | 0.023 | 0.073 | 0.089 | 0.09 | 0.023 | 0.028 | 0.03 |
| | Silty sand | 0.013 | 0.048 | 0.049 | 0.051 | 0.013 | 0.014 | 0.015 |
| | Mucky silty clay | 0.014 | 0.078 | 0.077 | 0.077 | 0.011 | 0.010 | 0.009 |
| $E_0$ (MPa) | Silt | 43.48 | 13.70 | 11.24 | 11.11 | 43.48 | 35.71 | 33.33 |
| | Silty sand | 76.92 | 20.83 | 20.41 | 19.61 | 76.92 | 71.43 | 66.67 |
| | Mucky silty clay | 71.43 | 12.82 | 12.99 | 12.99 | 90.91 | 100.00 | 111.11 |

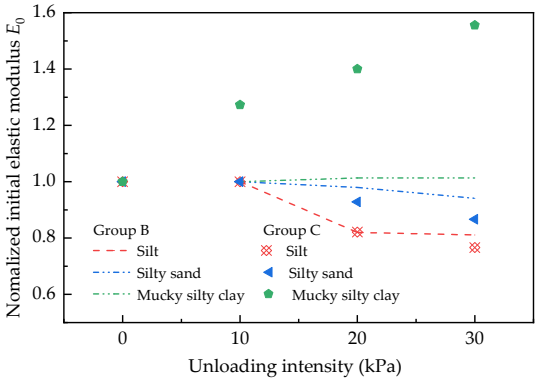


**Figure 9.** Normalized initial elastic modulus–unloading intensity relationship under different stress paths.

### *3.4. Small Strain Shear Stiffness*

Table 7 summarizes the shear wave velocity and small strain shear modulus as determined by the bender element test. The shear wave velocity and small-strain shear modulus measured during lateral unloading were lower than those measured during conventional stress paths and decrease as the unloading intensity increases. The shear wave velocity and modulus of elasticity measured in the lateral unloading–reloading stress path are similar to those measured under the conventional stress path but are greater than those measured in the unloading path.

**Table 7.** Experimental results of shear wave velocity and shear modulus under different stress paths.

| Properties | Soils | Stress Path | | | | | | |
|---|---|---|---|---|---|---|---|---|
| | | **A−0** | **B−1** | **B−2** | **B−3** | **C−1** | **C−2** | **C−3** |
| Shear wave velocity (m/s) | Silt | 241.5 | 209.9 | 207 | 204.3 | 240.1 | 238.1 | 235.3 |
| | Silty sand | 250.3 | 221.5 | 217.6 | 215.5 | 250 | 249.1 | 248.4 |
| | Mucky silty clay | 228.1 | 204.3 | 189.8 | 185.4 | 227.8 | 215.5 | 209.9 |
| Shear modulus (MPa) | Silt | 103.81 | 78.42 | 76.27 | 74.29 | 102.61 | 100.91 | 98.55 |
| | Silty sand | 111.52 | 87.33 | 84.28 | 82.66 | 111.25 | 110.45 | 109.83 |
| | Mucky silty clay | 92.61 | 78.42 | 64.12 | 61.18 | 92.37 | 82.66 | 78.42 |

Figure 10 illustrates the relationship between normalized small-strain shear modulus and unloading intensity for various stress paths. Unloading intensity had the greatest effect on the small strain shear modulus of mucky silty clay. When unloading intensity increased to 30 kPa, the small-strain shear modulus of Groups B and C decreased by 22% and 15%, respectively, indicating that the apparent structural damage of mucky silty clay was caused by unloading disturbance. In the unloading path, the small-strain shear moduli of silt and silty sand were similarly influenced by unloading intensity and were reduced by less than 5%. In the unloading–reloading path, the small-strain shear stiffness of the three soils remained essentially unchanged compared to the conventional triaxial path, but it significantly decreased as unloading intensity increased.

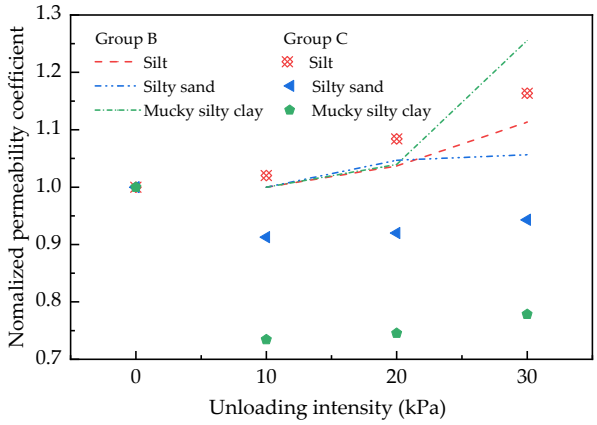


**Figure 10.** Normalized small-strain shear modulus–unloading intensity relationship of three soils under different stress paths.

### *3.5. Permeability Coefficient*

Table 8 summarizes the permeability coefficients of soil samples in the three different stress paths. The three soils had permeability coefficients ranging from large to small: silty sand, silt, and mucky silty clay. In the unloading path, silt and silty sand have higher permeability coefficients than that of the conventional path, whereas the permeability coefficient of mucky silty clay was lower than that of the conventional path, and gradually increased with increasing unloading intensity. In the unloading–reloading path, silt had a higher

permeability coefficient than that of the conventional path, while silty sand and mucky silty clay had a lower permeability coefficient than that of the conventional path. The variation curve of the normalized permeability coefficient with unloading intensity for three soils is shown in Figure 11. The permeability coefficient increased as unloading intensity increased. Unloading strength had the greatest effect on the permeability of mucky silty clay, but the overall permeability coefficient was small. In comparison to silty sand, the permeability of silt was more dependent on unloading intensity. The permeability coefficient increased by 11% and 16% in the unloading and unloading–reloading paths, respectively.

**Table 8.** Permeability coefficient of soil.

| Properties | Soils | Stress Path | | | | | | |
|---|---|---|---|---|---|---|---|---|
| | | **A−0** | **B−1** | **B−2** | **B−3** | **C−1** | **C−2** | **C−3** |
| Permeability coefficient ($\times 10^{-6}$ cm/s) | Silt | 188.50 | 188.84 | 195.81 | 210.24 | 192.31 | 204.32 | 219.32 |
| | Silty sand | 382.99 | 384.62 | 402.65 | 406.32 | 349.62 | 352.38 | 361.21 |
| | Mucky silty clay | 2.71 | 2.27 | 2.36 | 2.85 | 1.99 | 2.02 | 2.11 |

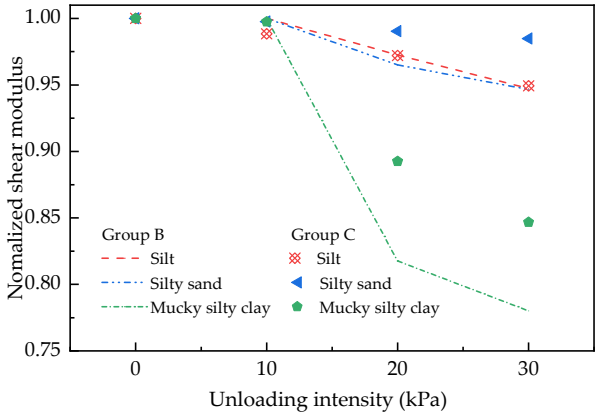


**Figure 11.** Normalized permeability coefficient-unloading intensity relationship of three soils in different stress paths.

## 4. Conclusions

A series of laboratory tests, namely, the CU triaxial, bender-element, and permeability tests of silt, mucky silty clay, and silty sand in the lateral unloading and unloading–reloading stress paths with different unloading intensity levels were carried out. The following conclusions could be drawn from the test results:

1. The lateral unloading and reloading of reconstituted Hangzhou soil containing silty particles reduced the shear strength and stiffness parameters. Ultimate deviator stress, effective cohesion, effective internal friction angle, initial elastic modulus, and small strain shear stiffness of soil decreased as unloading intensity increased. Unloading intensity had a more noticeable effect on the shear properties of silt and mucky silty clay.
2. In the unloading–reloading path, the shear strength and stiffness parameters of the silt, silty sand, and mucky silty clay were essentially consistent with those of conventional triaxial tests, indicating that the soil was not significantly disturbed. Increases in unloading intensity resulted in significant decreases in shear strength and stiffness parameters. The strength parameters of silt decreased the most (up to 7%), while the stiffness parameters of mucky silty clay decreased the most (up to 15%).
3. The permeability coefficients of all three types of reconstituted soils increased as unloading intensity increased, and the permeability coefficients of mucky silty clay and silt were more significantly affected.

**Author Contributions:** Conceptualization, C.X. and F.M.; methodology, C.X. and M.Z.; software, F.M. and Y.T.; validation, C.X. and F.M.; formal analysis, C.L.; investigation, C.X. and M.Z.; resources, C.X. and F.M.; data curation, F.M. and Y.T.; writing—original draft preparation, C.X.; writing—review and editing, C.X., F.M. and M.Z.; visualization, C.X. and F.M.; supervision, C.X. and F.M.; project administration, C.X., F.M. and M.Z.; funding acquisition, C.X., F.M. and M.Z. All authors have read and agreed to the published version of the manuscript.

**Funding:** This research was funded by China Postdoctoral Science Foundation grant number 2021T140475; Zhejiang Science and Technology Planning Project grant number 2013C31034; National Natural Science Foundation of China grant numbers 52090084, 52108329, and 52008263; and Shenzhen Science and Technology Program grant number KQTD20200909113951005.

**Institutional Review Board Statement:** Not applicable.

**Informed Consent Statement:** Not applicable.

**Data Availability Statement:** Data are contained in the article.

**Conflicts of Interest:** The authors declare no conflict of interest.

## References

1. Chen, X. Research on combined construction technology for cross-subway tunnels in underground spaces. *Engineering* **2018**, *4*, 103–111. [CrossRef]
2. Gong, X.; Zhang, X. Excavation collapse of Hangzhou subway station in soft clay and numerical investigation based on orthogonal experiment method. *J. Zhejiang Univ. SCIENCE A* **2012**, *13*, 760–767. [CrossRef]
3. Zhu, M.; Gong, X.; Gao, X.; Liu, S.; Yan, J. Remediation of damaged shield tunnel using grouting technique: Serviceability improvements and prevention of potential risks. *J. Perform. Constr. Facil.* **2019**, *33*, 04019062. [CrossRef]
4. Meng, F.; Chen, R.; Xu, Y.; Wu, K.; Wu, H.; Liu, Y. Contributions to responses of existing tunnel subjected to nearby excavation: A review. *Tunn. Undergr. Space Technol.* **2022**, *119*, 104195. [CrossRef]
5. Zheng, G.; Su, Y.; Diao, Y.; Zhao, Y.; Chen, H.; Huang, J. Field measurements and analysis of real-time capsule grouting to protect existing tunnel adjacent to excavation. *Tunn. Undergr. Space Technol.* **2022**, *122*, 104350. [CrossRef]
6. Yu, C. Numerical Analysis of Deep Foundation Pit Excavation Supported by Large Diameter Ring Beam. IOP Conference Series: Earth and Environmental Science. *IOP Publ.* **2019**, *242*, 062033. [CrossRef]
7. Zhu, M.; Chen, X.; Zhang, G.; Pang, X.; Su, D.; Liu, J. Parameter back-analysis of HS model for granite soil and its engineering applications. *Rock Soil Mech.* **2022**, 1–12. [CrossRef]
8. Lade, P.; Duncan, J. Stress-Path Dependent Behavior of Cohesionless soil. *J. Geotech. Engrg. Div.* **1976**, *102*, 42–48. [CrossRef]
9. Cui, Y.; Nguyen, X.; Tang, A.; Li, X. An insight into the unloading/reloading loops on the compression curve of natural stiff clays. *Appl. Clay Sci.* **2013**, *83*, 343–348. [CrossRef]
10. Zhou, Q.; Chen, X. Test research on typical mechanical characteristics of soft clay under lateral unloading condition. *Chin. J. Rock Mech. Eng.* **2009**, *28*, 2215–2221. [CrossRef]
11. Huang, W.; Li, J.; Lu, Y.; Li, D.; Mou, Y.; Wu, X.; Jiang, Z.; Li, Z. Mechanical Properties of Soft Soil considering the Influence of Unloading Stress Paths. *Adv. Civ. Eng.* **2021**, *2021*, 8813882. [CrossRef]
12. Huang, W.; Wen, K.; Liu, D.; Dong, Q.; Li, J.; Li, Y.; Li, L. Experimental study on influence of excess pore water pressure and unloading ratio on unloading mechanical properties of marine sedimentary soft soils. *Ocean Eng.* **2020**, *195*, 106680. [CrossRef]
13. Zheng, G.; Yan, Z.; Lei, H.; Wang, P. Experimental studies on unloading deformation properties of silty clay of first marine layer in Tianjin urban sea. *Rock Soil Mech.* **2008**, *29*, 1237–1242. [CrossRef]
14. Zheng, G.; Yan, Z.; Lei, H.; Wang, S. Experimental studies of unloading mechanical properties of silty clay of first marine layer in Tianjin city. *Rock Soil Mech.* **2009**, *30*, 1201–1208. [CrossRef]
15. Zhang, K.; Li, G.; Mei, X.; Du, W. Stress-deformation characteristics of silty soil based on K0 consolidation and drainage unloading stress path tests. *Chin. J. Geotech. Eng.* **2017**, *39*, 1182–1188. [CrossRef]
16. Ding, J.; Tian, B.; Huang, M.; Huang, H. Researches on mechanical properties of soil under conditions of excavation unloading in Guangzhou. In Proceedings of the 2017 2nd International Conference on Civil, Transportation and Environmental Engineering (ICCTE 2017), Shenzhen, China, 10–11 May 2017; Atlantis Press: Paris, France, 2017; pp. 83–95. [CrossRef]
17. Benz, T. *Small-Strain Stiffness of Soils and its Numerical Consequences*; University of Stuttgart, Institute of Geotechnical Engineering: Stuttgart, Germany, 2007.
18. Clayton, C. Stiffness at small strain: Research and practice. *Géotechnique* **2011**, *61*, 5–37. [CrossRef]
19. Vardanega, P.; Bolton, M. Stiffness of clays and silts: Normalizing shear modulus and shear strain. *J. Geotech. Geoenviron. Eng.* **2013**, *139*, 1575–1589. [CrossRef]
20. Carlton, B.; Pestana, J. A unified model for estimating the in-situ small strain shear modulus of clays, silts, sands, and gravels. *Soil Dyn. Earthq. Eng.* **2016**, *88*, 345–355. [CrossRef]

21. Prashant, A.; Bhattacharya, D.; Gundlapalli, S. Stress-state dependency of small-strain shear modulus in silty sand and sandy silt of Ganga. *Géotechnique* **2019**, *69*, 42–56. [CrossRef]
22. Hardin, B.; Richart, F., Jr. Elastic wave velocities in granular soils. *J. Soil Mech. Found. Div.* **1963**, *89*, 33–65. [CrossRef]
23. Vucetic, M.; Tabata, K. Influence of soil type on the effect of strain rate on small-strain cyclic shear modulus. *Soils Found.* **2003**, *43*, 161–173. [CrossRef]
24. Pyke, R. Nonlinear soil models for irregular cyclic loadings. *J. Geotech. Eng. Div.* **1979**, *105*, 715–726. [CrossRef]
25. Yuan, J.P.; Viet, N.H. Laboratory Study on Soil Shear Strength under Unloading Conditions. In Proceedings of the GeoHunan International Conference, Changsha, China, 9–11 June 2011; pp. 217–224. [CrossRef]
26. Kondner, R.L. Hyperbolic stress-strain response: Cohesive soils. *J. Soil Mech. Found. Div.* **1963**, *89*, 115–143. [CrossRef]